Research Journal of Applied Sciences, Engineering and Technology 4(13): 1940-1948, 2012
ISSN: 2040-7467

Submitted: February 16, 2012 Accepted: March 12, 2012 Published: July 01, 2012

Optimization Analysis of Discharged Gas Flow Duct in Gas Laser

[1]Jiang Fan and [2]He Hua
[1]School of Mechanical and Electric Engineering, Guangzhou University, Guangzhou, 510006, China
[2]Department of Mechanical and Electric Engineering, Bengbu College, Anhui 233030, China

Abstract: In order to obtain an accurately converged solution in a minimal amount of time, the porous medium model is used to replace a complicated 3D model to analyze flow field of gas duct, the results show that the height of discharge region, the expansion angle and the width of discharge region could affect the flow in the gas duct of CO_2 laser with pin-to-plate discharge. As the appropriate selection, the height of discharge region is 43.5 mm and the expansion angle is 8-10 degree, also, the length of gas duct is slightly larger (20-30 mm) than the width of the anode plate. The flow of the discharge region and stress on the cathode pin are influenced by arrangement of cathode pin, it concludes that the clutter arrangement is much better than the regular arrangement.

Key words: CO_2 laser, discharged gas flow duct, numerical simulation, porous medium model, structure optimization

INTRODUCTION

Since the first CO_2 laser has been invented, the CO_2 lasers become one of the most important lasers and have been developed rapidly due to its large power, high efficiency, steady output and excellent beam (Cheng and Xu, 2005; Xu *et al*., 2009). The discharged gas flow duct is key part of the transverse-flow CO_2 laser, its structure affects the volume of oscillation mode and fan capacity, could decide the residence time that work gas flow through the discharging region (Li and Huang, 2005). Over the past years, there have been many researches on the structure of discharging gas flow duct and some qualitative conclusions about its strucure parameters were obtained: when gas volume flow is constant, if throat size decreases, the flow velocity will increase; and as pressure is fixed, if throat size decreases, its resistance will increase and the flow velocity will reduce, that led to reduce of the volume flow, which is detrimental to the discharge (Li and Huang, 2005; Ukar *et al*., 2010). However, less data has been obtained on optimization analysis of the structure of gas flow duct in CO_2 laser with pin-to-plate discharge (one of the transverse-flow CO_2 laser).

On the structure of gas flow duct for transverse-flow CO_2 laser, the optimization analysis is a difficult task due to high cost of the traditional method and relatively long verification period. Finite volume method based Computational Fluid Dynamics (CFD) techniques can offer a cost-effect solution for flow strucutre optimization. The CFD model was used to optimize the discharge tube of fast-axial-flow CO_2 laser by Li (2009) At first, the theoretical governing equations were established including mass, momentum, energy conservation equations and three temperature model equations, then the geometric models were created by the software GAMBIT, after the flow field in discharge tube was analyzed by the software FLUENT, also the key factors were explained which has influence on the stability of glow discharge. Finally, two kind of new discharge tube strucute was designed for the fast-axial-flow CO_2 lasers. As results, both computational and expriments results show the better discharge performance is obtained for one of the new structure (Li, 2009). However, CO_2 laser with pin-to-plate discharge has many pins, which diameter is very small compared to the plate, thus the mesh size varied widely in CFD model and the computation become difficult, so a simplified method is needed to optimize the gas flow duct using by CFD model.

In this study, the porous medium model substitutes the pin region, then the CFD model with porous model is established to optimize the structure of gas flow duct. As results, the quantitative relationship is obtained between throat height and gas flow velocity when the volume flow is constant and the pressure is fixed. In addition, the influence is also discussed between cathode disctribution and its stress.

METHODOLOGY

Computational models: In Fig. 1, the actual physical model is shown to the gas flow duct in CO_2 laser with pin-

Corresponding Author: Jiang Fan, School of Mechanical and Electric Engineering, Guangzhou University, Guangzhou, 510006, China

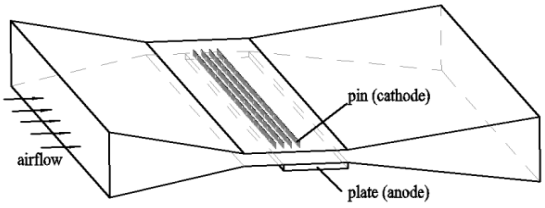

Fig. 1: Actual physical model of gas flow duct

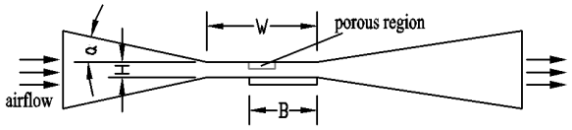

Fig. 2: 2D simplified model

to-plate discharge, there are small cathode pins in the gas flow. If we use this 3D model to numerical simulation, the mesh model will have many cells and the cells are mostly be tetrahedral and larger scale changes, which lead to lead to lower accuracy, longer computing time. In order to simplify the complicated 3D model, the porous medium model replaces the cathode pin region and the 2D longitudinal section is used as the computing domain, shown in Fig. 2. Therefore, the complex 3D problem becomes a simplified 2D problem, thus the compute time reduced significantly.

According to the simplified results and ignoring the impact of discharge energy, the CFD model of porous medium model establishes the standard fluid flow equations (including continuity equation, momentum equation), turbulence equations, they are expressed as following (Fauria and Rempel, 2011; Jiang *et al*., 2008a, b, 2009, 2010a, b).

- **Continuity equation:**

$$\nabla.(\rho\vec{v}) = 0 \tag{1}$$

where, ρ is fluid density, $\vec{v}$ is velocity vector.

- **Momentum conservation equation:**

$$\nabla.(\rho\vec{v}\vec{v}) = -\nabla p + \mu\nabla.[(\nabla\vec{v} + \nabla\vec{v}^T) - \frac{2}{3}\nabla.\vec{v}I] + \vec{G} + \vec{F} \tag{2}$$

where, p is the static pressure, μ is the viscosity, I is the unit tensor, $\vec{G}$ and $\vec{F}$ are the gravitational body force and external bofy force, respectively and $\vec{F}$ contains other model-dependent source terms such as porous-media and user-defined sources.

- The RNG k - ε model is closed the standard fluid flow equations, is expressed as following:

$$\frac{\partial}{\partial x_i}(\rho k u_i) = \frac{\partial}{\partial x_j}\left[\alpha_k(\mu + \frac{\rho C_\mu k^2}{\sigma_k \varepsilon})\frac{\partial k}{\partial x_j}\right] + G_k + G_b - \rho\varepsilon - Y_M + S_k \tag{3}$$

$$\frac{\partial}{\partial x_i}(\rho\varepsilon u_i)\frac{\partial}{\partial x_{ji}}\left[\alpha_\varepsilon(\mu + \frac{\rho C_\mu k^2}{\sigma_\varepsilon \varepsilon})\frac{\partial}{\partial x_j}\right] + C_{1\varepsilon}\frac{\varepsilon}{k}(G_k + C_{3\varepsilon}G_b) - C_{2\varepsilon}\rho\frac{\varepsilon^2}{k} - R_\varepsilon + S_\varepsilon \tag{4}$$

In these equations, k and ε are the turbulence kinetic energy and its dissipation rate, $G_k$represents the generation of turbulence kinetic energy due to the mean velocity gradient, G_b is the generation of turbulence kinetic energy due to buoyancy, Y_M represents the contribution of the fluctuating dilatation in compressible turbulence to the overall dissipation rate, The quantities α_k and α_ε are the inverse effective Prandtl numbers for k and ε , respectively. S_k and S_ε are user-defined source terms, $C_{1\varepsilon}$, $C_{2\varepsilon}$, $C_{3\varepsilon}$, C_μ, σ_k, σ_ε are constants, have the following default values, 1.42, 1.68, tanh|v/u| (where v is the component of the flow velocity parallel to the gravitational vector and u is the component of the flow velocity perpendicular to the gravitational vector), 0.0845, 1.0, 1.3, respectively.

- Porous media are modeled by an additional of a momentum source term to the standard fluid flow equations that recover the case of simple homogeneous porous media, the term is written as (Lipnikov *et al*., 2011):

$$S_i = -\left(\frac{\mu}{\alpha}v_i + C_2\rho|v|v_i\right) \tag{5}$$

where, α is the permeability, C_2 is the inertial resistance factor, α and C_2 are obtained by experiment, the computation method is as following (Parand *et al*., 2011).

$$\alpha = \frac{\mu}{\frac{p_1^2 - p_2^2}{2Lp_1u_1} - \frac{p_1u_1}{2L(p_1u_1 - p_2u_2)}\left(\frac{p_1}{u_2} - \frac{p_2}{u_2} - \frac{p_{01}^2}{p_1u_1} + \frac{p_{02}^2}{p_2u_2}\right)} \tag{6}$$

$$C_2 = \frac{RT}{2L(p_1u_1 - p_2u_2)}\left(\frac{p_1}{u_1} - \frac{p_2}{u_2} - \frac{p_{01}^2}{p_1u_1} + \frac{p_{02}^2}{p_2u_2}\right) \tag{7}$$

In above equations, p_1 and $u_1$are pressure and velocity of the first condition in front of porous region respectively; p_{01} is pressure of the first condition behind of porous region; p_2 and u_2 are pressure and velocity of the second condition in front of porous region respectively; p_{02} is pressure of the second condition behind of porous region; R is the thermodynamic constants, 8.314; T is temperature; L is length of porous region. Through the experiment, it obtained that the values of $\alpha$is 3.12E7 and C_2 is 0.739.

RESULTS AND DISCUSSION

Validation of the porous medium model calculation: As stated previously, the present study deals with the porous medium model instead of 3D complicated model, so two models are calculated and compared. Their parameters and mesh are listed in Table 1 and figured in Fig. 3a is 3D actual mesh model, Fig. 3b is porous medium mesh model). For these two models, the boundary conditions (inlet pressure is 13000 Pa) are same and the calculated results are shown in Fig. 4-7. The commercial code GAMBIT is used to create the mesh mode and FLUENT 6.3 is used to solve the above-mentioned equations.

In Fig. 4 and 6, a is contour results of 3D model and Fig. 6b is contour results of porous medium model.

Table 1: Validation model parameters

Parameter	3D model	The porous medium model
H_{duct}	45 mm	45 mm
W	162.5 mm	162.5 mm
α	9.08 mm	9.08 mm
B	100 mm	100 mm
L_{laser}	675 mm	675 mm
$L_{cathode}$	38.5 mm	38.5 mm
$L_{laserleft}$	211.25 mm	211.25 mm
H_{laser}	950	-
Cell number	983414	2280
Node number	232519	2420

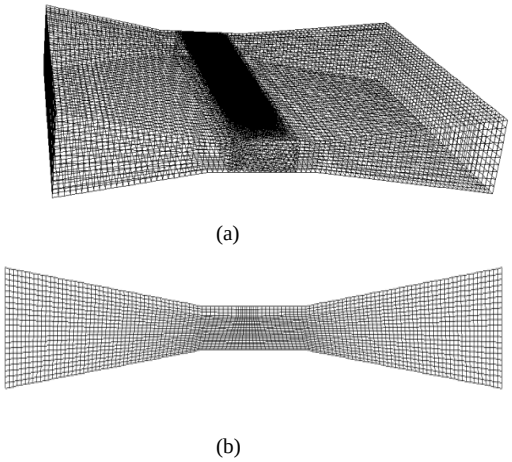

(a)

(b)

Fig. 3: Mesh model

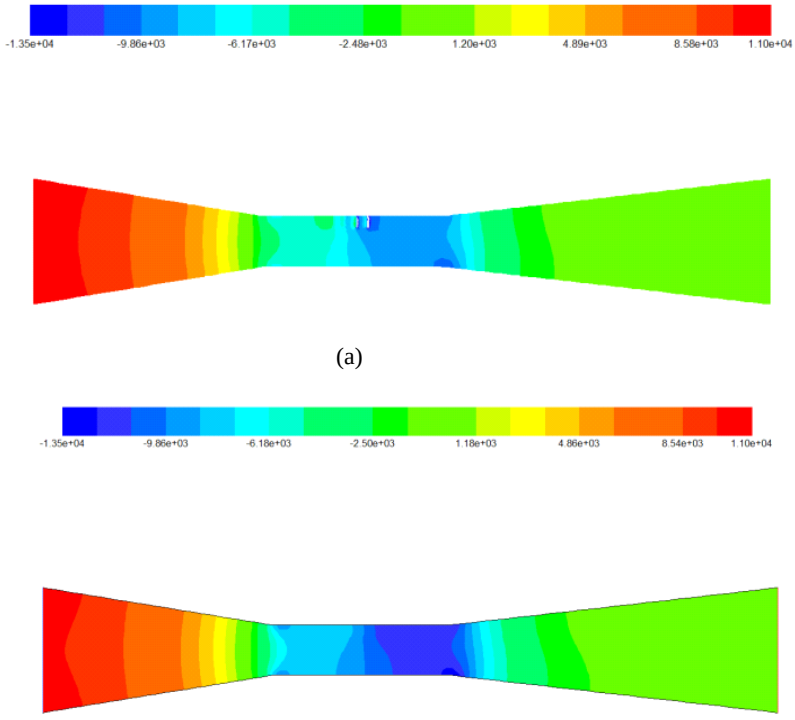

(a)

(b)

Fig. 4: Pressure contour comparation of longitudinal section

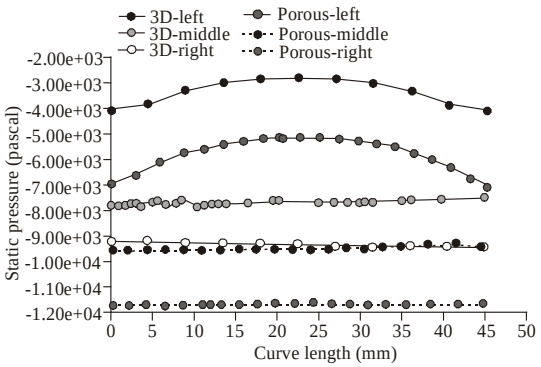

Fig. 5: Pressure comparation among three curves (left, middle, right of gas flow duct)

Figure 4 shows pressure contour at longitudinal section, their pressure distribution is almost same, in view of the cathodes blocking, the pressure at discharge region of the 3D actual model is less than that of the porous model. Detailed comparison is shown in Fig. 5, the pressure distribution of three curves in corresponding positions is plotted. Obviously, the pressure distribution curves of corresponding positions are similar, its pressure values have slightly differences that is 3 KPa on the curve of both sides (left and right) and is 1.6 KPa at the middle curve.

The velocity comparation of discharge gas flow duct is illustrated in Fig. 6-7, In Fig. 6, two velocity contours are very similar excluded a slightly different near the cathode pins. In 3D actual model, because of the arrangement of the cathode pin, the gas resistance is large and the velocity of 3D model is less than that of porous model. The detailed comparison of velocity on curves of three different positions is shown in Fig. 7. It can be seen that the different between two left curves is greater than that of middle and right curves.

Comparison between the 3D actual model and porous medium model shows that the porous medium model could take the place of 3D actual model, which simplify the mesh and greatly improve the computational efficiency.

Structure optimization of gas flow duct:

Influence of size H: To investigate on the influence of height of the gas flow duct to the velocity and volume flow of gas, five different calculation were analyzed with different duct height and the grid parameters, which shown in Table 2.

For fixed volume flow of inlet, the velocity distribution on central curves of different models is shown in Fig. 8 and as fixed pressure of inlet, the volume flow distribution on central curves of different models is shown in Fig. 9. The comprehensive comparison of these previous two cases is shown in Fig. 10.

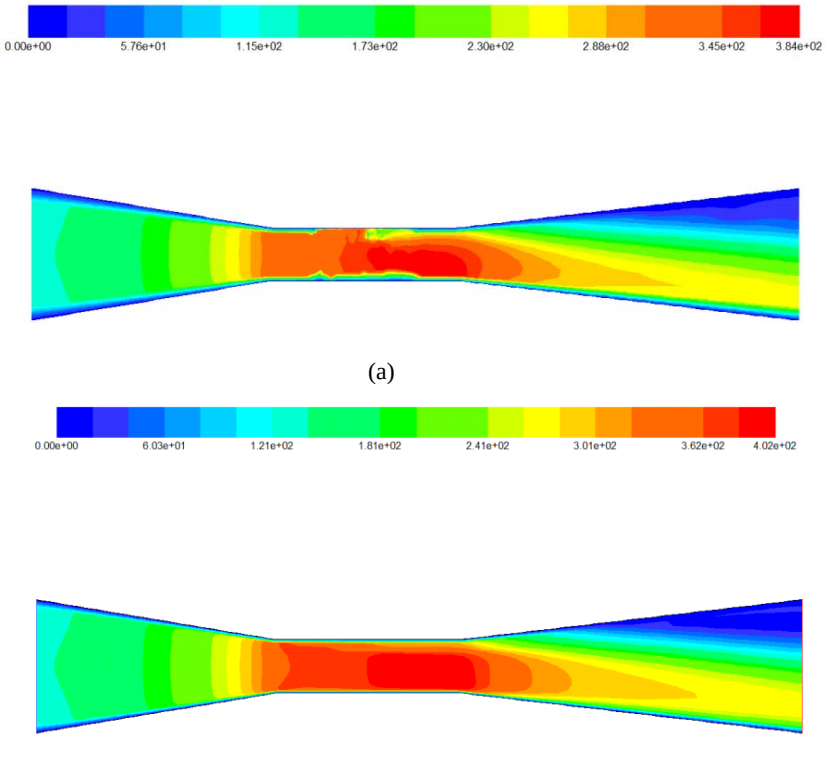

Fig. 6: Velocity contour comparation of longitudinal section

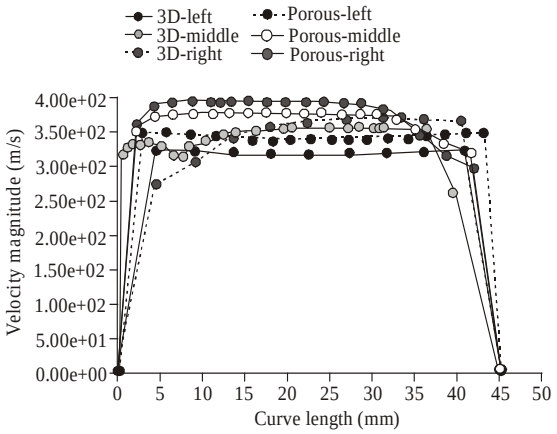

Fig. 7: Velocity comparation among three curves (left, middle, right of gas flow duct)

Table 2: Model parameters of different H

No.	H	Cells	Nodes
M1	35	3014	3190
M2	40	2772	2926
M3	45	2646	2794
M4	50	2520	2662
M5	55	2394	25

Figure 8 shows that velocity distribution along most of points of the central curve is horizontal, the below velocity increases linear mode as the boundary layer, the upper velocity has a stepped down as porous region. This figure also suggests that with the H increasing, flow velocity declines, where H in the range of 40-45 mm, the velocity difference is relatively large (10 m/s).

Figure 9 presents the volume flow distribution and variation of different H size. For different H, their volume flow distribution are similar; It is close to a horizontal line at the middle; For below, it increases linearly as the impact of the boundary layer; at the upper region of porous media, volume flow steps down, also it shows that with the H increases, volume flow also increased. When H increases by 5 mm, the volume flows evenly increases about 1.2 m^3/s.

Figure 10 shows that velocity variation and volume flow variation along with the H size variation, the change in the midpoint is plotted which combining of Fig. 8 and 9. When volume flow is constant, velocity decreases with H increasing. And if pressure different of two duct end is constant, volume flow will increases as H increases. When H is 43.5 mm, the velocity variation curve will intersect the volume flow variation curve. Then, the velocity is 73.58 m/s and volume flow is 11.83 m^3/s. Therefore, H is equal to 43.5 is the optimum value of H.

Influence of size α: Previous studies indicated that throat expansion at the upstream and downstream of gas duct helps to reduce pressure loss; on the contrary, when the expansion angle decreases, the structural size will increase for the pressure loss. Thus it's required an

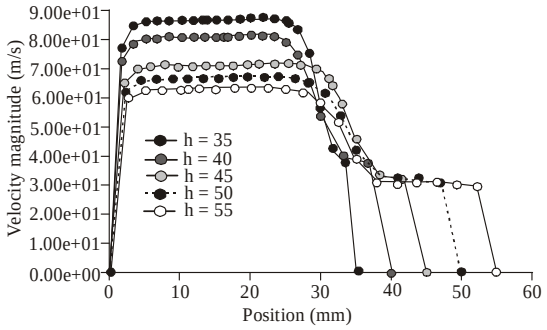

Fig. 8: Velocity comparison of different duct height

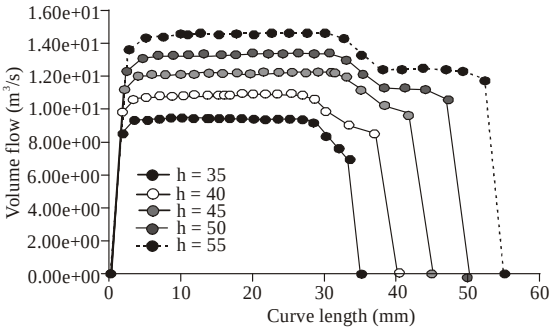

Fig. 9: Volume flow comparison of different duct height

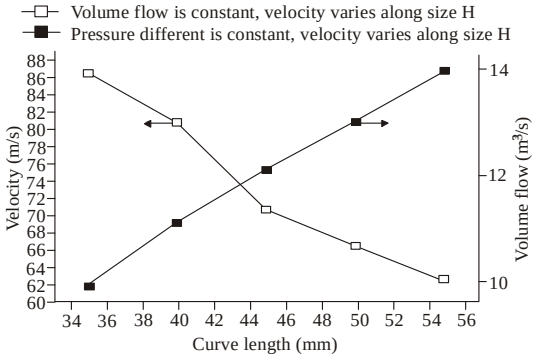

Fig. 10: Comprehensive comparison of two previous cases

Table 3: Model parameters of different α

No.	α	Cells	Nodes
M6	6	3318	3498
M7	8	2646	2794
M8	10	2226	2354
M9	12	1974	2090
M10	15	1722	1826

optimization of the expansion angle. Then five models with different expansion angle are calculated, the models parameters are shown in Table 3 and the results are shown in Fig. 11-12.

Figure 11 is velocity variation with different expansion angle on the central curve of gas duct. From Fig. 8, the velocity variation is similar. From the bottom to the top of gas duct, the velocity increases rapidly at the

Table 4: Model parameters of different W

No.	B	W	Cells	Nodes
M11	100	100	2478	2618
M12	100	130	2583	2728
M13	100	150	2646	2794
M14	100	180	2751	2904

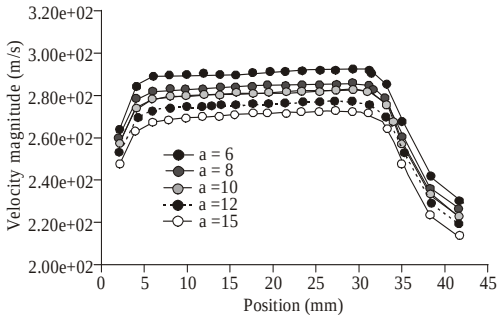

Fig. 11: Velocity variation of different expansion angle

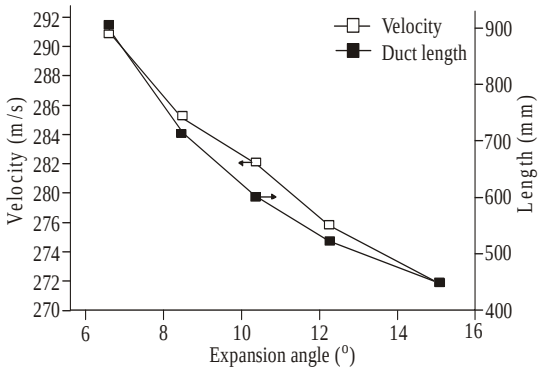

Fig. 12: Velocity and duct length variation with expansion angle

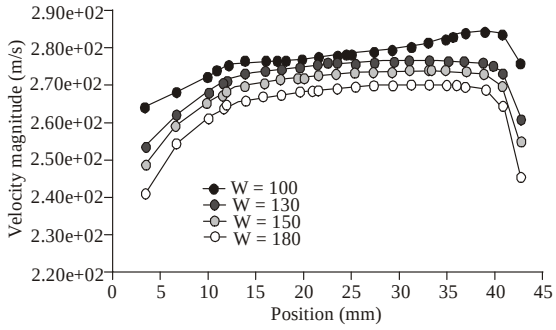

Fig. 13: Velocity curve of different W

beginning, slowly at the middle part and ladderly decreases in porous media. Also it shows when the expansion angle increases, the velocity reduces.

Figure 12 is the variation of velocity and duct length for the increasing expansion angle. As the expansion angle increases, the velocity and duct length are reduce. In general, for discharge region in the gas duct the higher gas velocity could help cooling. According to velocity curve, expansion angle should choose a small value.

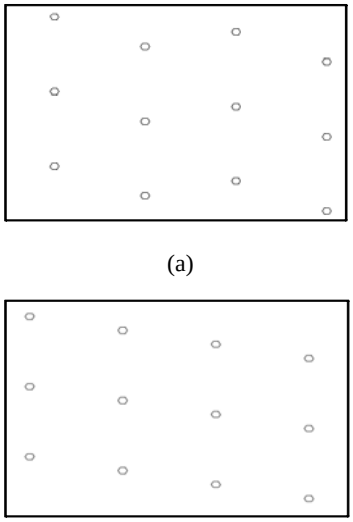

Fig. 14: Different arrangement of cathode pin

But if the expansion angle is very small, the size of gas duct will become too large, thus the appropriate degree of expansion angle is 8-10 degree.

Influence of size W: Width of discharge region is another important parameter that effect the total size of gas duct. Thus four models are created and calculated, the different model parameters are shown in Table 4 and the results are shown in Fig. 13.

From Fig. 13, as the width of discharge region increases, the flow resistance increases and the velocity decreases. The velocity curve W = 100 mm is the velocity distribution of the starting point at the section of the cathode pin where the width of the discharge region equals to the anode plate width. It can be seen that there are greater velocity fluctuations. If the fluctuation is small for the other velocity curves, it indicating the velocity is stable. It appears when the width of discharge region is greater than the width of anode plate. So it recommended that the width of discharge region is slightly greater (20-30 mm) than the width of the anode plate.

Arrangement analysis of cathode pin: The flow structure and stress of cathode pin are influenced by the arrangement of pins, thus the arrangement distribution is analyzed. Two models of different arrangement are created, they are shown in Fig. 14a is M15, the arrangement of cathode pin is clutter, Fig. 14b is M16, its arrangement is regular), their mesh parameters are shown in Table 5, the results are shown in Fig. 15-16.

Table 5: Model parameters of different cathodes distribution

No.	Cells	Nodes
M15	985463	232787
M16	975013	221513

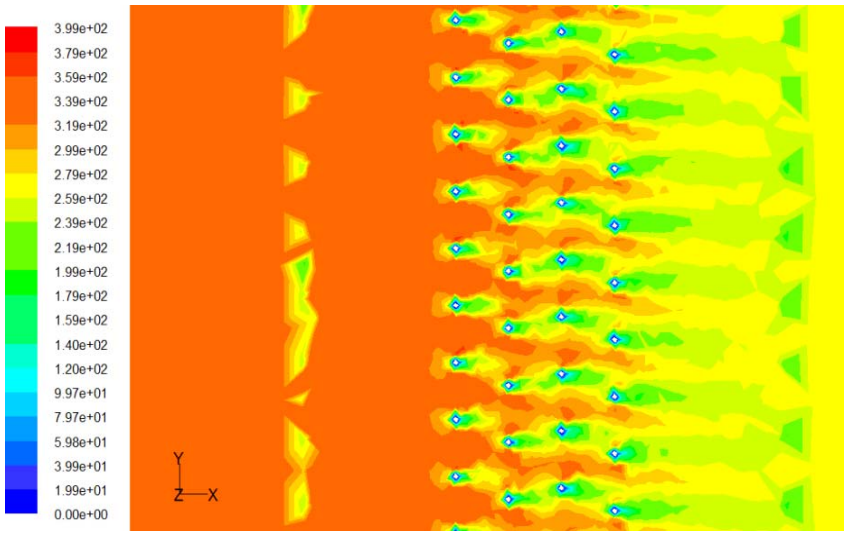

(a)

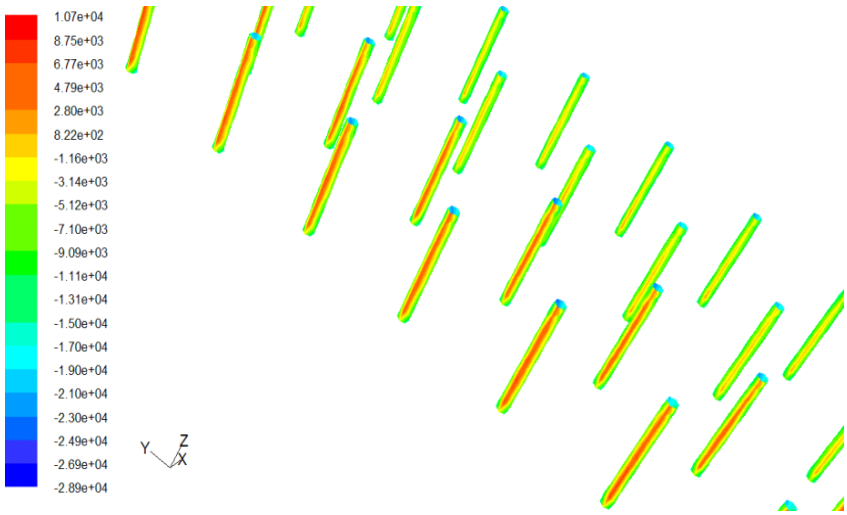

(b)

Fig. 15: Velocity and stress results of M15

In Fig. 15 and 16a is velocity contour on the level cross-section, Fig. 16b is stress contour on surface of cathode pins. The comparison is made on Fig. 15 and 16. When the arrangement varies of the cathode pin in the discharge region, the flow field and stress on cathode pin are also change. The arrangement of M15 has relatively smooth flow at discharge region. The velocity near the back of the cathode pins are higher, while the stress on the cathode pin is relatively small. Integrated, the arrangement of M15 is better than that of M16, that is to say, the clutter arrangement is better than the regular arrangement. Therefore the flow field and stress should be given full consideration when designing arrangement of the cathode pins.

CONCLUSION

- Calculation results show when use porous medium model instead of a complicated 3D model, the results are closed and keep the same trend, the porous medium could significantly reduce analysis time and improve analysis efficiency.
- Optimization analysis of gas duct structure shows that: the height of discharge region, the expansion angle and the width of discharge region could affect the flow inside of gas duct in CO_2 laser with pin-to-plate discharge. When the height of discharge region increases, the velocity decreases (the volume flow is constant) and the volume flow increases (inlet

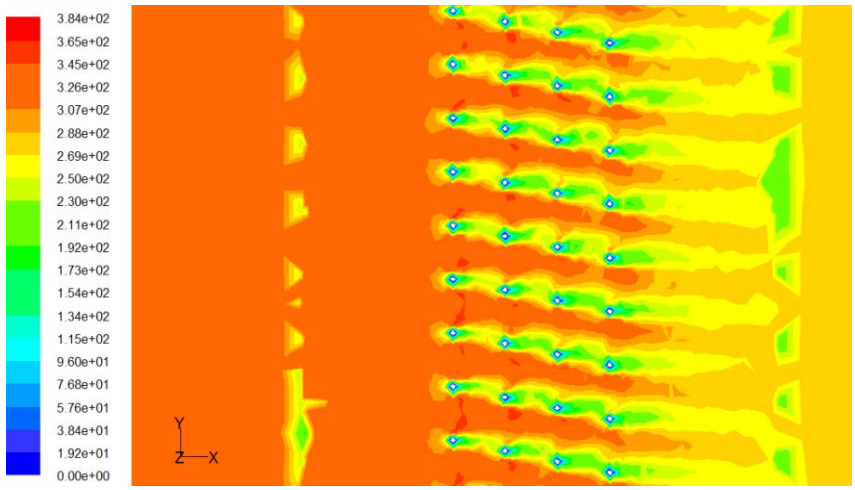

(a)

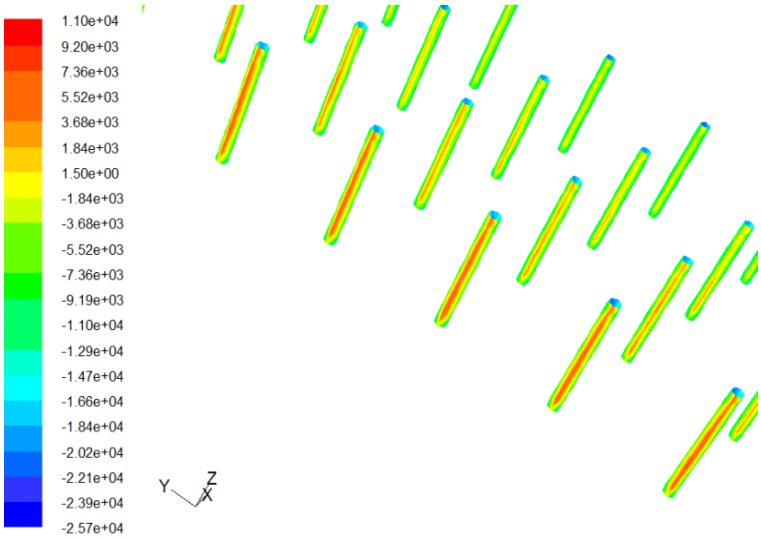

(b)

Fig. 16: Velocity and stress results of M16

pressure is constant). Thus the appropriate height is 43.5 mm. When the expansion angle increases, the velocity will decline and the length of gas duct will reduce, thus the appropriate angle is 8-10 degree. When the width of discharge region increases, the velocity will decrease and the stability of velocity will increase too; so it is appropriate to make the width of discharge region slightly larger (20-30 mm) than the width of the anode plate.

- Different arrangement of cathode pin impacts the flow of the discharge region and the stress on the cathode pin. In conclusion, the clutter arrangement (do not block each other) is much better than the regular arrangement.

REFERENCES

Cheng, C. and Z.S. Xu, 2005. Experiment determination of after-operating gas compositions in a transverse-flow CW high power CO_2 laser. Opt. Laser Technol., 37(4): 293-297.

Fauria, K.E. and A.W. Rempel, 2011. Gas invasion into water-saturated, unconsolidated porous media: Implications for gas hydrate reservoirs. Earth Planet. Sc. Lett., 312(1-2): 188-193.

Jiang, F., W.P. Chen and Y.Y. Li, 2008a. Spatial structure injection molding analysis of suspended bio-carriers. Mater. Sci. Forum, 575-578: 385-388.

Jiang, F., W.P. Chen and Y.Y. Li, 2008b. Numerical evaluation of spatial structure of suspended bio-Carriers. J. South China Uni. Technol., 37(12): 75-79.

Jiang, F., X.C. Liu and C. Wang, 2009. Numerical simulation of soot particle flow indoor of automobile. Proceedings of the 3rd International Conference on Mechanical Engineering and Mechanics, 1: 1010-1015.

Jiang, F., J. Yu and Z.W. Liang, 2010a. New blood vessel robot design and outside flow field characteristic. Appl. Mech. Mater., 29-32: 2490-2495.

Jiang, F., J. Yu and Z.M. Xiao, 2010b. Outside flow field characteristic of biological carriers. Adv. Mat. Res., 113-114: 276-279.

Li, Q., 2009. Computational fluid dynamics modeling of discharge tubein Fast-axial-flow CO_2 Laser. Ph.D. Thesis, Huazhong University of Seience and Technology, Wuhan, China.

Li, S.M. and W.L. Huang, 2005. Principle and Design of Laser Devices. National Defence Industry Press, Beijing, China.

Lipnikov, K., J.D. Moulteon and D. Svyatskly, 2011. Adaptive strategies in the multilevel multiscale mimetic (M3) method for two-phase flows in porous media. Multiscale Model. Sim., 9(3): 991-1016.

Parand, K., S. Abbasbandy, S. Kazem and A.R. Rezaei, 2011. Comparison between two common collocation approaches based on radial basis functions for the case of heat transfer equations arising in porous medium. Commun. Nonlinear Sci., 16(3): 1396-1407.

Ukar, E., A. Lamikiz, L.N. Lopez de Lacalle, D. del Pozo and J.L. Arana, 2010. Laser polishing of tool steel with CO_2 laser and high-power diode laser. Int. J. Machine Tools Manufacture, 50(1): 115-125.

Xu, Y.G., Y.D. Li, B. Zhang, T. Feng and Y. Qiu, 2009. Theoretical study of misalignment analysis of the holophote and self-phase locking of axisymmetrical-structural CO_2 laser. Opt. Lasers Eng., 47(7-8): 782-792.